Numerical Simulation of Flow Field at Entrance of Nozzle Bank in Chemical Laser

Wang Jie[1,2] Weng Chunsheng[2] Yin Yanhua[1] Guo Jianzeng[1] Yan Feixue[1]

[1] *Handan Purification Equipment Research Institute, Handan, Hebei* 056027, *China*
[2] *National Key Laboratory of Transient physics, Nanjing University of Science and Technology, Nanjing, Jiangsu* 210094, *China*

Abstract In order to investigate the characteristic of the flow field at the entrance of the nozzle bank in a chemical laser, a physical and numerical model which is compatible with the flow was established. The model based on experimental equipment contained two types of nozzle bank with three nozzles and four nozzles, respectively. The two-dimensional viscous conservation element and solution element (CE/SE) method was used to calculate the numerical model. The results show that the CE/SE method can simulate the flow process of the high temperature burned gas effectively. The parameters gained from the simulation accord with the experimental data as the flow reaches stable. To a single nozzle, the related parameters(such as pressure and velocity) distribution in the flow field is symmetrical, which can be extended to the nozzle bank with more nozzles.

Key words chemical laser; flow characteristic; conservation element and solution element method; nozzle bank
OCIS 140.1550; 140.3290

化学激光器喷管列阵入口流场的数值模拟

王 杰[1,2] 翁春生[2] 尹燕华[1] 郭建增[1] 颜飞雪[1]

([1] 邯郸净化设备研究所, 河北 邯郸 056027; [2]南京理工大学瞬态物理国家重点实验室, 江苏 南京 210094)

摘要 为了研究化学激光器喷管列阵入口流场的变化特性,建立了适合于该流场特点的数学物理模型。该模型以化学激光器实验装置为基础,其喷管列阵分别由 3 个和 4 个单独的喷管构成。应用二维黏性守恒元与求解元(CE/SE)方法对该数值模型进行了计算模拟。结果表明,CE/SE 方法能有效地模拟该流场中高温燃气的流动过程;流场达到稳定后计算得到的相关参数与实验结果基本吻合;对单一的喷管而言,流场中的相关参数(如压力、速度等)分布具有一定的对称性,其结果可以扩展至由更多单一喷管组成的喷管列阵。

关键词 化学激光器; 流动特性; 守恒元与求解元方法; 喷管列阵
中图分类号 T248.5 **文献标识码** A **doi**: 10.3788/LOP48.101402

1 Introduction

The combustor and the nozzle bank are very important modules for a HF/DF chemical laser. The combustor′s purpose is to produce fluorine atoms. The fluorine atoms, F, are produced in a combustor from the reaction of excess NF_3 or F_2 and C_2H_4 or other hydrocarbon fuels(but D_2 for HF chemical laser) with helium or nitrogen diluents. The nozzle bank located at the exit of the combustor is made up of many tiny nozzles. The fluorine atoms are expanded through nozzle bank and inject into the cavity where they are mixed with supersonic streams of D_2 (H_2) and He. The theory and experiment data show that the parameters, such as fluorine atoms flow rate, stagnation pressure, and stagnation temperature at the entrance of nozzle bank, have effect on efficiency and output power of the laser.

Numerical simulation as a research technique had been applied to many problems in a chemical laser. Munson[1] constructed a model to predict the parameters, such as combustor plenum pressure, stagnation temperature, core temperature and average temperatures of the vessel walls in a chemical laser combustor. McGregor *et al.*[2] developed a method based on the direct simulation Monte Carlo(DSMC) approach to

收稿日期: 2011-03-11; **收到修改稿日期**: 2011-05-03; **网络出版日期**: 2011-08-30
作者简介: 王 杰(1982—), 博士,主要从事化学激光器方面的研究。E-mail: wangjie_24@163.com

screen injector concepts for high-energy chemical lasers. The method involved modeling the associated complex three-dimensional, reacting, multispecies flow fields, which enabled screening the high-performance injector concepts. Tang *et al.*[3] gave a new method to solve the multi-component chemical equilibrium flows with elements distributing equations and thermodynamic calculation of chemical equilibrium in a DF chemical laser combustion chamber. Hua *et al.*[4] used a compressible scaling (CS) method to simulate the nozzle flow field and optical flow field of the 3-slot continuous wave (CW) HF chemical laser. Jia *et al.*[5] developed a computer program to solve the coupled flow-optics interaction problem. Li *et al.*[6,7] used a two-step combustion method in gas film cooling gain generator. In this paper, we established a chemical laser model with three or four nozzles in the nozzle bank and used the CE/SE method to simulate the flow field at the entrance of nozzle bank. We attempt to obtain the related parameters and the flow characteristic, which are the groundwork for the simulation of the flow field in a chemical laser in the future.

2 Physical model

Figure 1 is the schematic of physical model. The fluorine atoms produced in the combustor are expanded through the nozzle bank and inject into the cavity. The insert placed between combustor and nozzle bank can protect the nozzles from being ablated or eroded by the high temperature and pressure gas. We assumed the entrance of nozzle bank to be the domain $ABCD$. In this domain, the combustion reaction has already reached equilibrium, and the products are F, HF, CF_4, N_2, He, etc. Also, the equilibrium compositions of combustion reaction in a chemical laser are calculated by the minimum Gibbs′ free energy method.

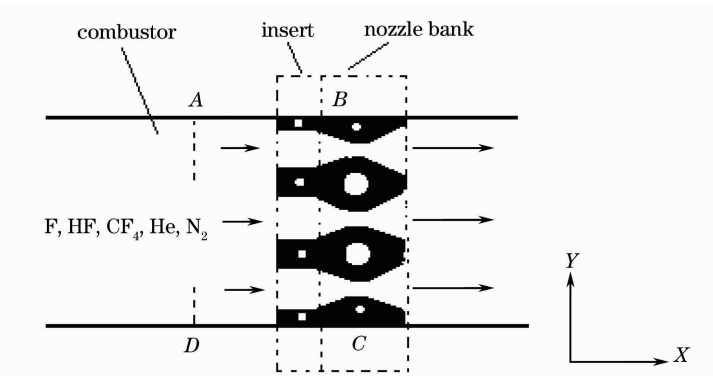

Fig.1 Schematic of physical model

The lengths of AD and AB are 0.1 and 0.025 m. The width of insert is 0.01 m. In this paper, we consider two nozzle bank models with three nozzles and four nozzles, respectively. The width of a single nozzle entrance in two models is 0.0112 or 0.0084 m. All nozzles are well-proportioned located between the region AB and DC.

3 Numerical model

3.1 Governing equations

In order to simplify the process of simulation, it is assumed that 1) the gas is idea gas; 2) the boundary walls of the gas flow are adiabatic; 3) the turbulence and dissipation can be neglected.

Based on these assumptions mentioned above, we obtained a dimensionless form of the two-dimensional (2D) unsteady Navier-Stokes equations:

$$\frac{\partial \boldsymbol{U}}{\partial t}+\frac{\partial(\boldsymbol{F}-\boldsymbol{F}_v)}{\partial x}+\frac{\partial(\boldsymbol{G}-\boldsymbol{G}_v)}{\partial y}=0, \tag{1}$$

with

$$\boldsymbol{U}=[\rho,\ \rho u,\ \rho v,\ \rho E]^{\mathrm{T}},$$

$$\boldsymbol{F}=[\rho u,\rho u^2+p,\rho v u,(\rho E+p)u]^{\mathrm{T}},$$

$$\boldsymbol{F}_v=\frac{1}{Re}[0,\tau_{xx},\tau_{xy},u\tau_{xx}+v\tau_{xy}+q_x]^{\mathrm{T}},$$

$$\boldsymbol{G}=[\rho v,\rho u v,\rho v^2+p,(\rho E+p)v]^{\mathrm{T}},$$

$$\boldsymbol{G}_v=\frac{1}{Re}[0,\tau_{yx},\tau_{yy},u\tau_{yx}+v\tau_{yy}+q_y]^{\mathrm{T}},$$

where ρ, p, u, and v represent the density, pressure, x- and y- velocity components, respectively. The total internal energy E is given by

$$E=\frac{p}{\rho(\gamma-1)}+\frac{1}{2}(u^2+v^2), \tag{2}$$

where γ is the ratio of specific heat which is taken as a constant.

The normal stresses (τ_{xx}, τ_{yy}), shear stresses (τ_{xy}, τ_{yx}), and energy diffusion fluxes (q_x, q_y) are given by

$$\tau_{xx}=\mu\Big[2\frac{\partial u}{\partial x}-\frac{2}{3}\Big(\frac{\partial u}{\partial x}+\frac{\partial v}{\partial y}\Big)\Big],\quad \tau_{yy}=\mu\Big[2\frac{\partial v}{\partial y}-\frac{2}{3}\Big(\frac{\partial u}{\partial x}+\frac{\partial v}{\partial y}\Big)\Big],$$

$$\tau_{xy}=\tau_{yx}=\mu\Big(\frac{\partial u}{\partial y}+\frac{\partial v}{\partial x}\Big),\qquad q_x=\frac{\mu}{Pr}\frac{1}{Ec}\frac{\partial T}{\partial x},\qquad q_y=\frac{\mu}{Pr}\frac{1}{Ec}\frac{\partial T}{\partial y},$$

where T and μ represent the temperature and viscosity, respectively. Re, Ec, and Pr are Reynolds, Eckert and Prandtl constants, respectively.

3.2 Numerical method

We used the CE/SE method for the 2D unsteady Navier-Stokes equations. The CE/SE method first proposed by Chang[8] had been used to obtain highly accurate numerical solutions for flow problems involving shocks, detonation waves, rarefaction waves, vortices, etc[9~11]. The CE/SE method is different from previous numerical method in nature and its basic idea is global and local flux conservation in a space-time domain. The method treats the space and time as a single entity, does not need a Riemann solver, and has high precision.

According to Chang's idea[8], let x, y, and t be the coordinates of three-dimensional (3D) Euclidean space E_3. The Navier-Stokes Eq. (11) in space-time E_3 can be converted into the integral form as

$$\oint_{S(V)}\boldsymbol{h}\cdot\mathrm{d}\boldsymbol{V}=0, \tag{3}$$

where $\boldsymbol{h}=(\boldsymbol{F}-\boldsymbol{F}_v,\boldsymbol{G}-\boldsymbol{G}_v,\boldsymbol{U})$ is the flux density vectors in space-time of mass, x-momentum component, y-momentum component, energy, respectively, and $S(V)$ is the boundary of an arbitrary space-time region V in E_3. The whole calculation region is divided into non-overlapping conservation elements (CEs) and solution elements (SEs). Applying the CE/SE theory[8,12] to quadrilateral meshes, we can obtain the 2D viscous CE/SE scheme as

$$\begin{aligned}\boldsymbol{U}_{i,j}^{n}=&\frac{1}{4}\Big[\Big(\boldsymbol{U}+\frac{\Delta x}{4}\boldsymbol{U}_x\Big)-\frac{\Delta t}{4}\Big(\boldsymbol{G}_y-\frac{8}{\Delta x}\boldsymbol{F}-\boldsymbol{F}_x-\frac{2\Delta t}{\Delta x}\boldsymbol{F}_t\Big)\Big]_{i-1/2,j}^{n-1/2}+\\&\frac{1}{4}\Big[\Big(\boldsymbol{U}-\frac{\Delta x}{4}\boldsymbol{U}_x\Big)-\frac{\Delta t}{4}\Big(\boldsymbol{G}_y+\frac{8}{\Delta x}\boldsymbol{F}-\boldsymbol{F}_x+\frac{2\Delta t}{\Delta x}\boldsymbol{F}_t\Big)\Big]_{i+1/2,j}^{n-1/2}+\\&\frac{1}{4}\Big[\Big(\boldsymbol{U}+\frac{\Delta y}{4}\boldsymbol{U}_y\Big)-\frac{\Delta t}{4}\Big(\boldsymbol{F}_x-\boldsymbol{G}_y-\frac{8}{\Delta y}\boldsymbol{G}-\frac{2\Delta t}{\Delta y}\boldsymbol{G}_t\Big)\Big]_{i,j-1/2}^{n-1/2}+\\&\frac{1}{4}\Big[\Big(\boldsymbol{U}-\frac{\Delta y}{4}\boldsymbol{U}_y\Big)-\frac{\Delta t}{4}\Big(\boldsymbol{F}_x-\boldsymbol{G}_y+\frac{8}{\Delta y}\boldsymbol{G}+\frac{2\Delta t}{\Delta y}\boldsymbol{G}_t\Big)\Big]_{i,j+1/2}^{n-1/2}+\\&\boldsymbol{I}_{i,j+1/2}^{n-1/2}+\boldsymbol{I}_{i,j-1/2}^{n-1/2}+\boldsymbol{I}_{i+1/2,j}^{n-1/2}+\boldsymbol{I}_{i-1/2,j}^{n-1/2},\end{aligned} \tag{4}$$

where $\boldsymbol{I}_{i,j\pm1/2}^{n-1/2}$ and $\boldsymbol{I}_{i\pm1/2,j}^{n-1/2}$ are the space-time density integral flux of diffusion items. $\boldsymbol{F}_t$, $\boldsymbol{G}_t$, $\boldsymbol{F}_x$, and $\boldsymbol{G}_y$ are the functions of $\boldsymbol{U}$, $\boldsymbol{U}_x$, and $\boldsymbol{U}_y$. The expressions $\boldsymbol{U}_x$ and $\boldsymbol{I}_y$ can be found in Ref. [11].

4 Results and discussion

Figure 2 is the schematic of computational domain. Since the flow field is assumed to 2D symmetry, we just simulate half the region ($OAKLMFEGHPO$). The spatial domains are divided into 0.1 mm × 0.1 mm uniform quadrilateral cells. For the walls of AK, KL, LM, FE, EG, and GH, we use a new wall boundary that the shear stress exerted on the fluid by a wall is modeled as a source term as a part of local space-time flux conservation[13]. We use symmetric boundary condition for OP, non-reflecting boundary condition for MF and HP. The parameters of AO are gained by the measurement data and the calculation results. At the beginning of simulation, the pressure, temperature, and density are same as environment parameters. The length in Fig. 2 is dimensionless, and the reference length is the length of OP (X_0). Moreover, the following parameters in all figures are non-dimensional. The reference pressure (p_0), temperature (T_0), and density (ρ_0) are the parameters of environment. The reference velocity is $\sqrt{RT_0}$, and the reference time is $X_0/\sqrt{RT_0}$.

The pressure histories are shown in Fig. 3. The real line denotes simulation results, and the pentacle denotes experimental results. The pressure measure nod is near to the solid wall at $X=0.6$. We just choose several pressure points in the experiment compared with the simulation results. From Fig. 3, we can see that the simulation pressure accords well with the experimental results. The pressure is 5.24 as the flow field reaches stable. In fact, there are some random fluctuations in the field before the pressure reaching stable. However, the last stable case is consistent with the experimental results.

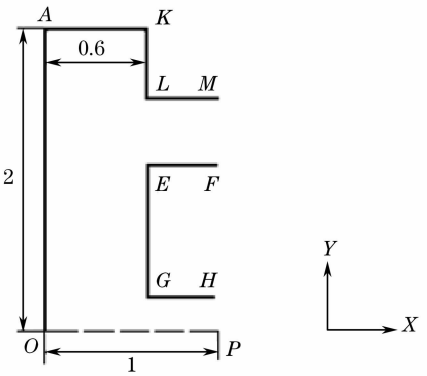

Fig. 2 Schematic of the computational domain

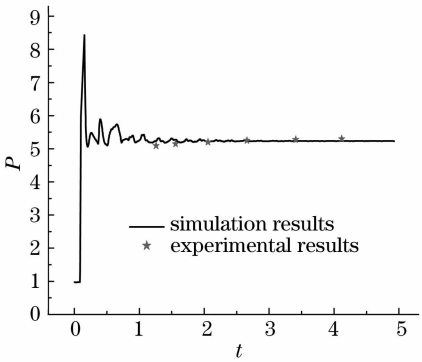

Fig. 3 Pressure history as a function of time

The pressure contours at the entrance of nozzle bank with three nozzles are shown in Fig. 4. Three figures represent the pressure diversification from $t = 0.18$ to $t = 4.25$. The burned gas diffuses to $X = 0.78$ at $t = 0.18$, and we can see two compression waves at $X = 0.44$. The compression waves are formed because the burned gas flow reflects from the solid wall KL and EG. The pressure distribution is such as in Fig. 4(b) at $t = 0.27$. Two isolated compression waves interact and connect together. At $t = 4.25$, the compression waves vanish, some suction waves appear and spread from left to right. Also, we can see that the pressure contours are symmetrical for a single nozzle.

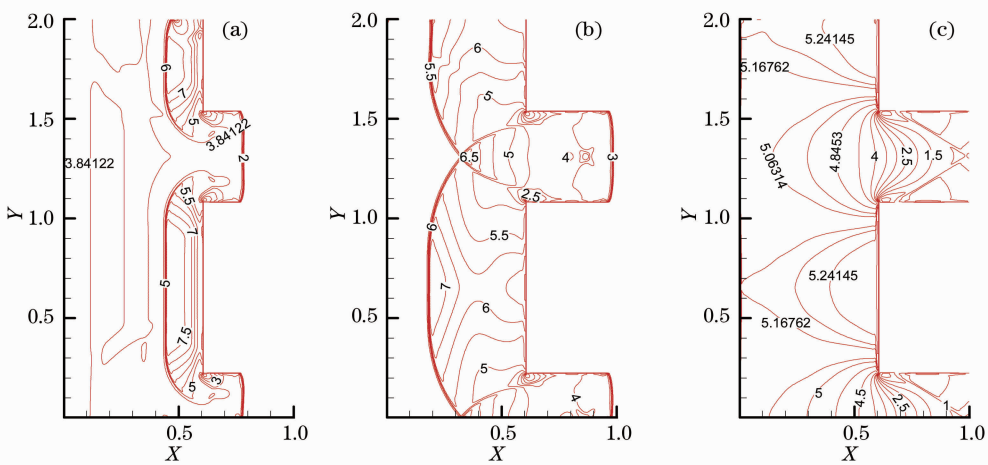

Fig. 4 Pressure contours at different times. (a) $t = 0.18$; (b) $t = 0.27$; (c) $t = 4.25$

The pressure contours at the entrance of nozzle bank with four nozzles are given in Fig. 5. The pressure distributions correspond the times of $t = 0.18$, 0.27 and 4.22, respectively. By contrasting Fig. 5 with Fig. 4, we

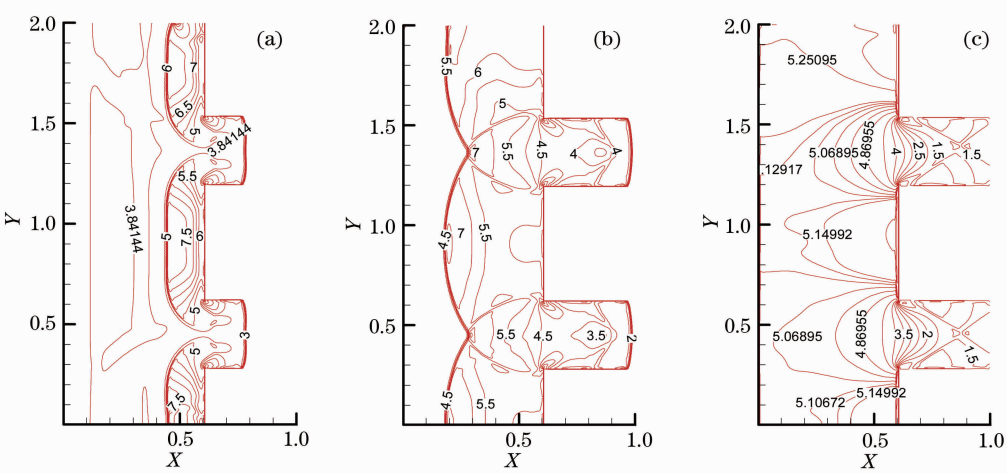

Fig. 5 Pressure contours at different times. (a) $t = 0.18$; (b) $t = 0.27$; (c) $t = 4.22$

can find that the rules of pressure diversification are similar. Three compression waves are formed at $X=0.44$ because the burned gas flows reflect from three solid walls at $t=0.18$. As the time going, three isolated compression waves spread to left, and then interact or connect. At $t=4.22$, the gas flow has reached stable and the pressure distribution becomes equable, correspondingly.

Figure 6 is the contours of velocity along Y-axis at $t=5.55$. Figures 6(a) and (b) represent the velocity field at the entrance of nozzle bank with three nozzles and four nozzles, respectively. The contours are similar in shape by contrasting two figures. Some velocity in figures is negative, because the direction of velocity is in opposition with the Y-axis. Moreover, the velocity along Y-axis is maximum near the corner of the wall, so the corner is eroded firstly by high temperature gas, which accords with the experimental results. In order to prevent the right-angle corner being eroded easily by the burned gas, the smooth corner is applied frequently.

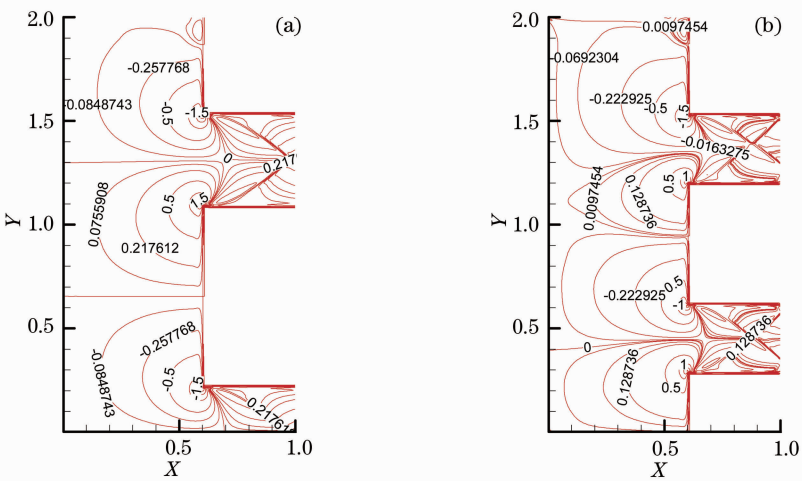

Fig. 6 Contours of velocity along Y-axis at $t=5.55$. (a) Three nozzles; (b) four nozzles

Figure 7 is the curves of velocity along Y-axis at $X=0.6$. Four curves in Fig. 7(a) show the distribution of the velocity along Y-axis at $t=0.00$, 0.27, 1.17, and 4.25. The velocity is zero at the time of $t=0$. As the time going, the velocity field becomes stable gradually. The velocity distribution changes little from $t=1.17$ to $t=4.25$. Also, we can see that the velocity distribution is centrosymmetric from $Y=1.09$ to $Y=1.54$. It is the width of a single nozzle fitly. The same rule exists in Fig. 7(b) from $Y=0.30$ to $Y=0.64$ and from $Y=1.20$ to $Y=1.54$.

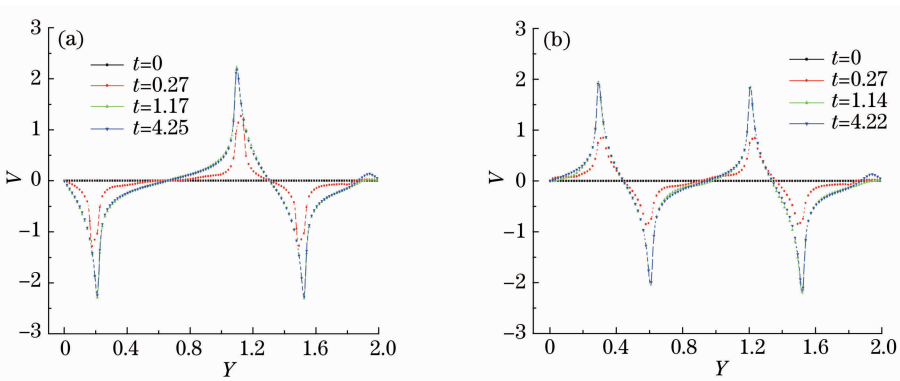

Fig. 7 Curves of velocity along Y-axis at $X=0.6$. (a) Three nozzles; (b) four nozzles

After the insert being improved, the pressure contours are given in Fig. 8. The right-angle of the insert is whittled to 45° bevel, and the hypotenuse is 2 mm. Because of the symmetry of the flow, only half of the nozzle field is shown in figures. The pressure contours are similar while you see half of the nozzle flow in Fig. 4, but the flow can reach stable faster. So the bevel is propitious to the stability of the flow field, more research about the insert will be done in the future.

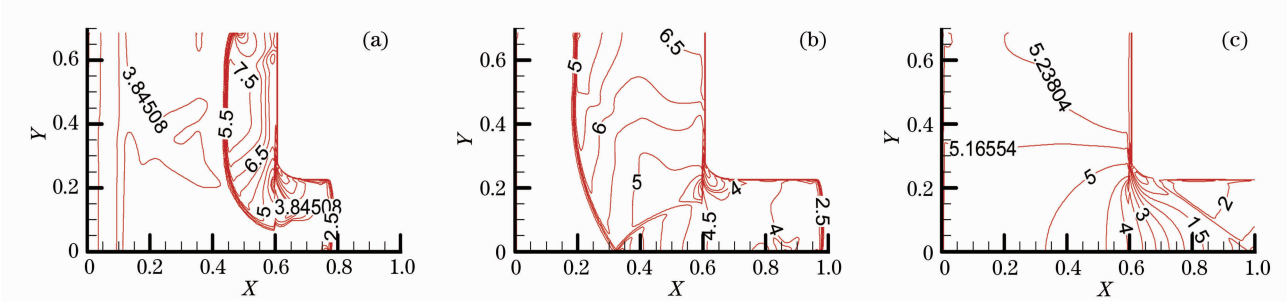

Fig. 8 Pressure contours at different times. (a) $t = 0.18$; (b) $t = 0.24$; (c) $t = 3.38$

5 Conclusions

We established a numerical model, and used the 2D CE/SE method to simulate the flow field at the entrance of the nozzle bank in a chemical laser. The results indicate that the CE/SE method enables simulating the flow process of the burned gas effectively. Before the flow field reaching stable, some compression waves appear and spread along with the time going. The corner of the solid walls will be ablated or eroded firstly because of the larger velocity along Y-axis in a certain extent. The related parameters distribution in the flow field is symmetrical, so we can extend the results to the nozzle bank with more nozzles. Applying the results, more simulation works in a chemical laser will be developed in the future.

References

1 A. K. Munson. A model predictor for chemical laser combustors[R]. *AIAA Paper*, 2001-2868

2 R. D. McGregor, D. E. Haflinger, P. D. Lohn *et al*.. Modeling of HF chemical laser flow fields using the Direct Simulation Monte Carlo method[R]. *AIAA Paper*, 1992-2980

3 Tang Litie, Zhuo Haitao, Lu Qisheng. Numerical solution to multi-component chemical equilibrium flows in DF chemical laser combustion chamber[J]. *High Power Laser and Particle Beams*, 2005, **17**(11): 1625～1629
唐力铁,卓海涛,陆启生. DF 激光器燃烧室反应流场的一种新的计算求解方法[J]. 强激光与粒子束, 2005, **17**(11): 1625～1629

4 Hua Weihong, Jiang Zongfu, Zhao Yijun. Numerical study of the 3-slot CW HF chemical laser[J]. *Chinese J. Lasers*, 1997, **24**(3): 221～227
华卫红, 姜宗福, 赵伊君. 三喷管型连续波 HF 化学激光器性能的数值模拟研究[J]. 中国激光, 1997, **24**(3): 221～227

5 Jia Shuqing, Huai Ying, Jin Yuqi *et al*.. Coupling simulation of flow and optical fields in supersonic chemical oxygen-iodine lasers[J]. *Laser & Optoelectronics Progress*, 2009, **46**(9): 59～63
贾淑芹, 怀 英, 金玉奇 等. 超音速化学氧碘激光器的流场与光场耦合仿真[J]. 激光与光电子学进展, 2009, **46**(9): 59～63

6 Li Lan, Hua Weihong, Yuan Shengfu *et al*.. Theoretical investigation of nozzle with helium film injection at the converge section in CW DF/HF chemical laser[J]. *Chinese J. Lasers*, 2009, **36**(2): 362～366
李 兰,华卫红,袁圣付 等. 连续波 DF/HF 化学激光器收缩段氦气膜注入式新型喷管的理论研究[J]. 中国激光, 2009, **36**(2): 362～366

7 Li Lan, Yuan Shengfu, Hua Weihong *et al*.. Numerical study of two-step combustion′s application in gas film cooling gain generator[J]. *Chinese J. Lasers*, 2010, **37**(8): 1967～1971
李 兰,袁圣付,华卫红 等. 两步燃烧法应用于气膜冷却式增益发生器流场数值模拟研究[J]. 中国激光, 2010, **37**(8): 1967～1971

8 S. C. Chang. The method of space-time conservation element and solution element——A new approach for solving the Navier-Stokes and euler equations[J]. *J. Computational Physics*, 1995, **119**: 295～324

9 Wang Jie, Weng Chunsheng. Numerical calculation of 3-D flow outside multi-tube pulse detonation engine[J]. *Chinese J. Theoretical and Applied Mechanics*, 2009, **41**(6): 835～841
王 杰,翁春生. 多管脉冲爆轰发动机外三维流场的数值计算[J]. 力学学报, 2009, **41**(6): 835～841

10 Chunsheng Weng, J. P. Gore. A numerical study of two- and three-dimensional detonation dynamics of pulse detonation engine by the CE/SE method[J]. *Mechanica Sinica*, 2005, **21**(1): 32～39

11 Z. C. Zhang, S. T. Yu. A generalized space-time CE-SE method for the euler equations on quadrilateral and hexagonal meshes[R]. *AIAA Paper*, 2001-2592

12 Y. H. Guo, T. H. Andrew, J. Wu *et al*.. Extension of CE-SE method to 2D viscous flows[R]. *AIAA Paper*, 2000-3385

13 S. C. Chang, Z. C. Zhang, S. T. Yu *et al*.. A unified wall boundary treatment for viscous and in-viscid flows in the CE/SE method [R]. NASA/TM-2000-210517